2 Carbon Fibre Composites: Deformation Micromechanics Analysed using Raman Spectroscopy

Robert J Young

School of Materials, University of Manchester, Manchester, M13 9PL, UK

2.1. Introduction

In the quest to understand reinforcement by high performance fibres, such as carbon fibres, the development of the subject of composite micromechanics is traced from its earliest roots. It is shown first how, employing concepts introduced by Kelly, it is possible through the use of shear-lag theory to predict the distribution of stress and strain in a single discontinuous fibre in a low-modulus matrix. For a number of years the shear-lag approach could only be used theoretically as there were no techniques available to monitor the stresses within a fibre in a resin. It is then shown that the advent of Raman spectroscopy and the discovery of stress-induced Raman bands shifts in reinforcing fibres, has enabled us to map out the stresses in individual fibres in a transparent resin matrix, and thereby both test and develop Kelly's pioneering analytical approach.

2.2. Fibre Reinforcement – Theory

2.2.1. Composite micromechanics

Interest in the mechanics of fibre reinforcement can be traced back to the first uses of high-modulus fibres to reinforce a low modulus matrix. A useful relationship developed to describe this reinforcement is the so-called 'rule of mixtures' in which, for stress parallel to the fibre direction, the Young's modulus of a composite E_c consisting of infinitely-long aligned fibres is given by an equation of the form

$$E_c = E_f V_f + E_m V_m \tag{2.1}$$

where E_f and E_m are the Young's modulus of the fibre and matrix and V_f and V_m are the volume fraction of the fibre and matrix respectively (Young and Lovell, 2011). This equation captures the essence of fibre reinforcement and is found to work well in the specific conditions outlined above when high modulus fibres are incorporated into low modulus matrix materials. Since the strain in the fibre and matrix are the same, the stress in the fibres is much higher than that in the matrix - hence the fibres take most of the load and so reinforce the polymer matrix.

O. Paris (Ed.), *Structure and Multiscale Mechanics of Carbon Nanomaterials*,
CISM International Centre for Mechanical Sciences
DOI 10.1007/ 978-3-7091-1887-0_2 © CISM Udine 2016

In reality, however, composites do not consist of infinitely-long aligned fibres and are not always stressed parallel to the fibre direction. The full analysis of the situation in reality is the subject of many composites textbooks (Hull and Clyne, 1996; Gibson, 2012). The deformation of composites containing fibres of finite length deformed axially has been considered by a number of authors including Krenchel (1964). In addition he also analysed the situation with fibres aligned randomly in plane and also randomly in three dimensions (Krenchel, 1964).

The problem of transfer of stress from the matrix to a fibre and the subsequent variation of stress along a fibre of finite length in a matrix was first tackled properly by Kelly (1966) in his classical text, 'Strong Solids'. This ground breaking work involved both the revival of the shear lag concept of Cox (1952) and considerable intuition on his part. Indeed, in the introductory text to Chapter V of Strong Solids (Kelly, 1966) he makes the following statement. "*In this chapter we will discuss firstly how stress can be transferred between the matrix and fibre. This will be done in a semi-intuitive fashion since it is a difficult problem to solve exactly*".

Kelly's analysis became the foundation of a new research field known as 'composite micromechanics'. It will be shown how it gave us the framework for the study of fibre reinforcement at both a theoretical and practical level, also enabling us to use the approach to tailor the properties of fibre-matrix interfaces in composites.

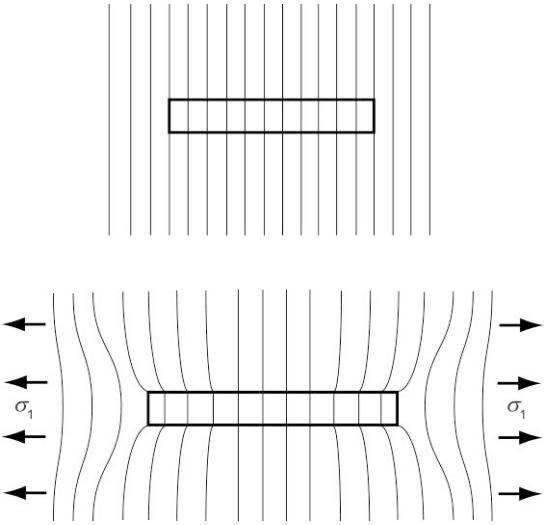

Figure 2.1. Deformation patterns for a discontinuous high-modulus fibre in a low-modulus polymer matrix. The top diagram shows the situation before deformation and the bottom diagram shows the effect of the application of a tensile stress, σ_1, parallel to the fibre. (Adapted from Young and Lovell, 2011 with permission from CRC Press).

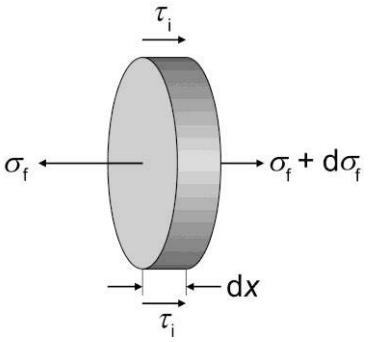

Figure 2.2. Balance of stresses acting on an element of the fibre of thickness d*x* in the composite. (Adapted from Young and Lovell, 2011 with permission from CRC Press).

2.2.2. Discontinuous Fibres

In the case of discontinuous fibres reinforcing a composite matrix, stress transfer from the matrix to the fibre takes place through a shear stress at the fibre-matrix interface as shown in Figure 2.1. It is envisaged that parallel lines perpendicular to the fibre can be drawn from the matrix through the fibre before deformation. When the system is subjected to an axial stress σ_l parallel to the fibre axis, the lines become distorted since the Young's modulus of the matrix is much lower than that of the fibre. This induces a shear stress at the fibre/matrix interface and the axial stress in the fibre builds up from zero at the fibre ends to a maximum value in the middle of the fibre. The assumption of uniform strain means that in the middle of the fibre the strain in the fibre equals that in the matrix, if the fibre is long enough. Since the fibres generally have a much higher Young's modulus than the matrix, the fibres then carry most of the stress (and hence load) in the composite – this is essentially how composites work (Kelly and Macmillan, 1986).

It is now necessary to introduce the concept of interfacial shear stress (Kelly, 1966). The relationship between the interfacial shear stress τ_i near the fibre ends and the fibre stress σ_f can be determined by using a balance of the shear forces at the interface and the tensile forces in a fibre element, as shown in Figure 2.2. The main assumption is that the force due to the shear stress τ_i at the interface is balanced by the force due to the variation of axial stress $d\sigma_f$ in the fibre such that

$$2\pi r \tau_i dx = -\pi r^2 d\sigma_f \tag{2.2}$$

and so

$$\frac{d\sigma_f}{dx} = -\frac{2\tau_i}{r} \tag{2.3}$$

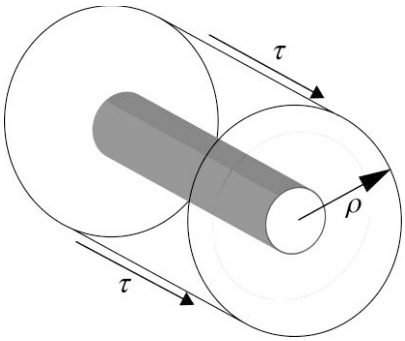

Figure 2.3. Model of a fibre undergoing deformation within a resin used in shear-lag theory. The shear stress τ acts at a radius ρ from the fibre centre. (Adapted from Young and Lovell, 2011 with permission from CRC Press).

2.2.3. Elastic Stress Transfer

The behaviour of a discontinuous fibre in a matrix can be modelled using shear lag theory, developed initially by Cox (1952) to model the mechanical properties of paper. It is assumed in the theory that the fibre is surrounded by a cylinder of resin extending to a radius ρ from the fibre centre, as show in Figure 2.3. In this model it is assumed that both the fibre and matrix deform elastically and that the fibre-matrix interface remains intact. If u is the displacement of the matrix in the fibre axial direction at a radius ρ then the shear strain γ at that position is be given by

$$\gamma = \frac{\mathrm{d}u}{\mathrm{d}\rho} \tag{2.4}$$

The shear modulus of the matrix is defined as $G_\mathrm{m} = \tau/\gamma$, hence it follows that

$$\frac{\mathrm{d}u}{\mathrm{d}\rho} = \frac{\tau}{G_\mathrm{m}} \tag{2.5}$$

The shear force per unit length carried by the matrix cylinder surface is $2\pi\rho\tau$ and is transmitted to the fibre surface though the layers of resin and so the shear stress at radius ρ is given by

$$2\pi\rho\tau = 2\pi r\tau_\mathrm{i} \tag{2.6}$$

and so

$$\tau = \left(\frac{r}{\rho}\right)\tau_\mathrm{i} \tag{2.7}$$

It follows using Equation (2.5), that

$$\frac{\mathrm{d}u}{\mathrm{d}\rho} = \left(\frac{r}{\rho}\right)\frac{\tau_\mathrm{i}}{G_\mathrm{m}} \tag{2.8}$$

It is possible to integrate this equation using the limits of the displacement at the fibre surface ($\rho = r$) of $u = u_\mathrm{f}$ and the displacement at $\rho = R$ of $u = u_\mathrm{R}$

$$\int_{u_\mathrm{f}}^{u_\mathrm{R}} \mathrm{d}u = \left(\frac{r\tau_\mathrm{i}}{G_\mathrm{m}}\right)\int_{r}^{R}\frac{\mathrm{d}\rho}{\rho} \tag{2.9}$$

hence

$$u_\mathrm{R} - u_\mathrm{f} = \left(\frac{r\tau_\mathrm{i}}{G_\mathrm{m}}\right)\ln\left(\frac{R}{r}\right) \tag{2.10}$$

These displacements can be converted into strain since the fibre strain e_f and matrix strain e_m can be approximated as $e_\mathrm{f} \approx \mathrm{d}u_\mathrm{f}/\mathrm{d}x$ and $e_\mathrm{m} \approx \mathrm{d}u_\mathrm{R}/\mathrm{d}x$. It should be noted that this shear-lag analysis is not rigorous, as shown by Nairn (1997), but it serves as a simple illustration of the process of stress transfer from the matrix to a fibre in a short-fibre composite. In addition, τ_i is given by Equation (2.3) and so differentiating Equation (2.10) with respect to x leads to

$$e_\mathrm{f} - e_\mathrm{m} = -\frac{r^2}{2G_\mathrm{m}}\left(\frac{\mathrm{d}^2\sigma_\mathrm{f}}{\mathrm{d}x^2}\right)\ln\left(\frac{R}{r}\right) \tag{2.11}$$

Furthermore, multiplying through by E_f gives

$$\frac{\mathrm{d}^2\sigma_f}{\mathrm{d}x^2} = -\frac{n^2}{r^2}\left(\sigma_\mathrm{f} - e_\mathrm{m}E_\mathrm{f}\right) \tag{2.12}$$

where

$$n = \sqrt{\frac{2G_\mathrm{m}}{E_f\ln(R/r)}}$$

This differential equation has the general solution

$$\sigma_\mathrm{f} = E_\mathrm{f}e_\mathrm{m} + C\sinh\left(\frac{nx}{r}\right) + D\cosh\left(\frac{nx}{r}\right)$$

where C and D are constants of integration. Now, equation (2.12) can be simplified and solved by double differentiation of the general solution, if it is assumed that the boundary conditions are that there is no stress transmitted across the fibre ends, i.e. if

$x = 0$ in the middle of the fibre where $\sigma_f = E_f e_m$ then $\sigma_f = 0$ at $x = \pm l/2$ where l is the length of the fibre. This leads to $C = 0$ and comparing terms gives

$$D = -\frac{E_f e_m}{\cosh(nl/2r)}$$

Finally, the equation for the distribution of fibre stress as a function of distance, x along the fibre is

$$\sigma_f = E_f e_m \left[1 - \frac{\cosh(nx/r)}{\cosh(nl/2r)}\right] \tag{2.13}$$

2.2.4. Interfacial shear stress

It is possible, now, to determine the distribution of interfacial shear stress along the fibre using Equation (2.3) which by differentiation of Equation (2.13) leads to

$$\tau_i = \frac{n}{2} E_f e_m \frac{\sinh(nx/r)}{\cosh(nl/2r)} \tag{2.14}$$

It is convenient to introduce the concept of fibre aspect ratio s (= $l/2r$) which is dimensionless so that the two above equations can be rewritten as

$$\sigma_f = E_f e_m \left[1 - \frac{\cosh\left(ns\frac{2x}{l}\right)}{\cosh(ns)}\right] \tag{2.15}$$

for the axial fibre stress and as

$$\tau_i = \frac{n}{2} E_f e_m \frac{\sinh\left(ns\frac{2x}{l}\right)}{\cosh(ns)} \tag{2.16}$$

for the interfacial shear stress. The effect of the different parameters upon the variation of stress in a fibre is demonstrated in Figure 2.4 for different values of the product ns. It can be seen from this figure that the fibre is most highly stressed, i.e. the most efficient fibre reinforcement is obtained, when the product ns is high. This therefore implies that a high aspect ratio s is desirable along with a high value of n, for the best reinforcement.

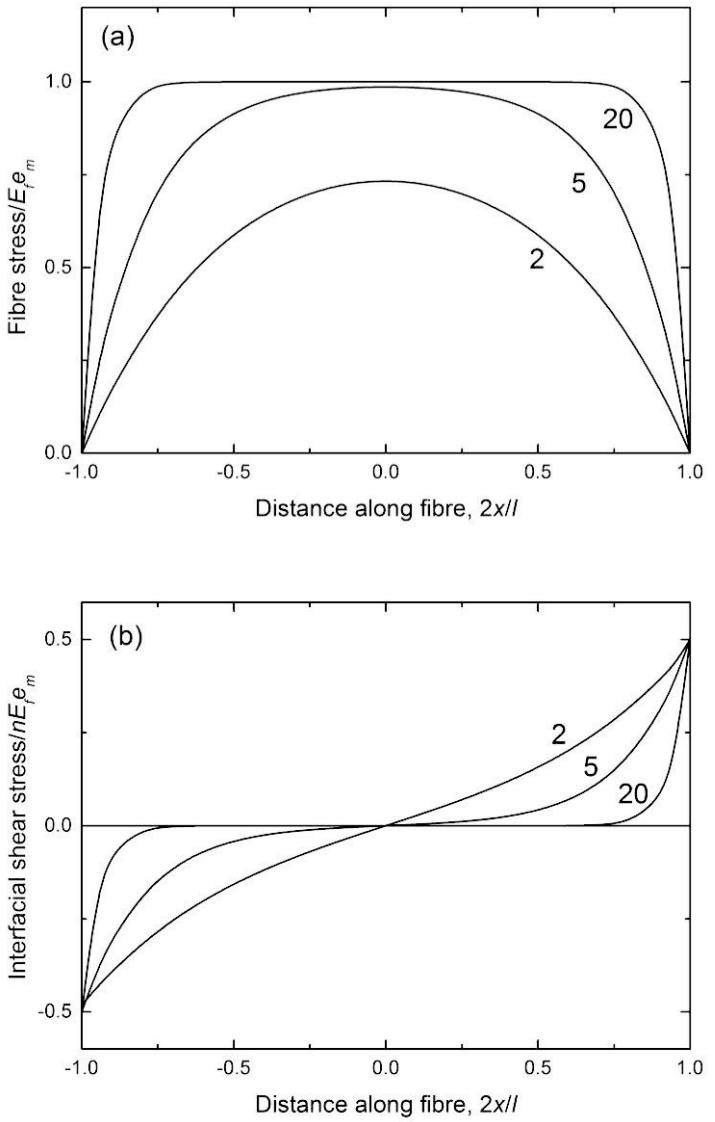

Figure 2.4. (a) Predicted variation of fibre stress with distance along the fibre for a short fibre in matrix. (b) Predicted variation of interfacial shear stress with distance along the fibre for a short fibre. The values of the product *ns* are indicated in each case. (Adapted from Young and Lovell, 2011 with permission from CRC Press).

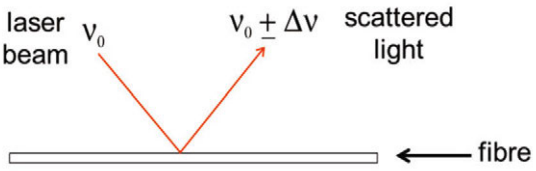

Figure 2.5. Schematic diagram of the Raman scattering from a single fibre.

2.3. Fibre Reinforcement – Experiment

2.3.1. Raman Spectra of Carbon Fibres

Following this original theoretical determination of stresses in discontinuous fibres, researchers had to rely upon it for the analysis of the micromechanics of composites, since there were initially no experimental methods available to measure local fibre stress or strain. Experimental measurement of the fibre stress and strain in discontinuous fibres in a composite under stress has now become available through the use of Raman spectroscopy (Huang and Young, 1994). This is shown schematically in Figure 2.5 where a sample such as a carbon fibre is irradiated with a laser beam of frequency, ν_0. Most of the light is scattered at the same frequency (or energy) with a small amount scattered at different frequencies of $\pm \Delta\nu$. This is the Raman scattered light and many high-performance fibres have well-defined Raman spectra (Young, 1995). Moreover when the fibres are deformed in a Raman spectrometer large stress-induced band shifts are obtained as the result of the externally applied stress distorting the covalent bond in the fibre backbone. This type of behaviour has been found for fibres such as Kevlar, polyethylene and PBO (Young, 1995). This is not so surprising since the excellent mechanical properties of high performance fibres are the result to the covalent bond in the backbone taking the load during deformation. Indeed, carbon fibres are found to behave in a similar manner.

Raman spectra are shown in Figure 2.6 for PAN- and pitch-based carbon fibres. In all cases the spectra exhibit the same appearance, that is, four well-resolved bands, namely D (~1330 cm^{-1}), G (~1580 cm^{-1}), D' (~1620 cm^{-1}) and 2D (~2660 cm^{-1}) along with additional weaker features. Figure 2.6 shows spectra for the fibres both untreated and treated with oxygen plasma to improve fibre-matrix adhesion (Montes-Morán and Young, 2002a). No differences were observed in Raman band positions and widths after the plasma treatment of the fibres but the intensity ratio of the two first-order bands D and G is always higher after the plasma treatment, showing that this treatment introduces defects and functionality into the fibre surface which we will see results in better fibre-matrix adhesion.

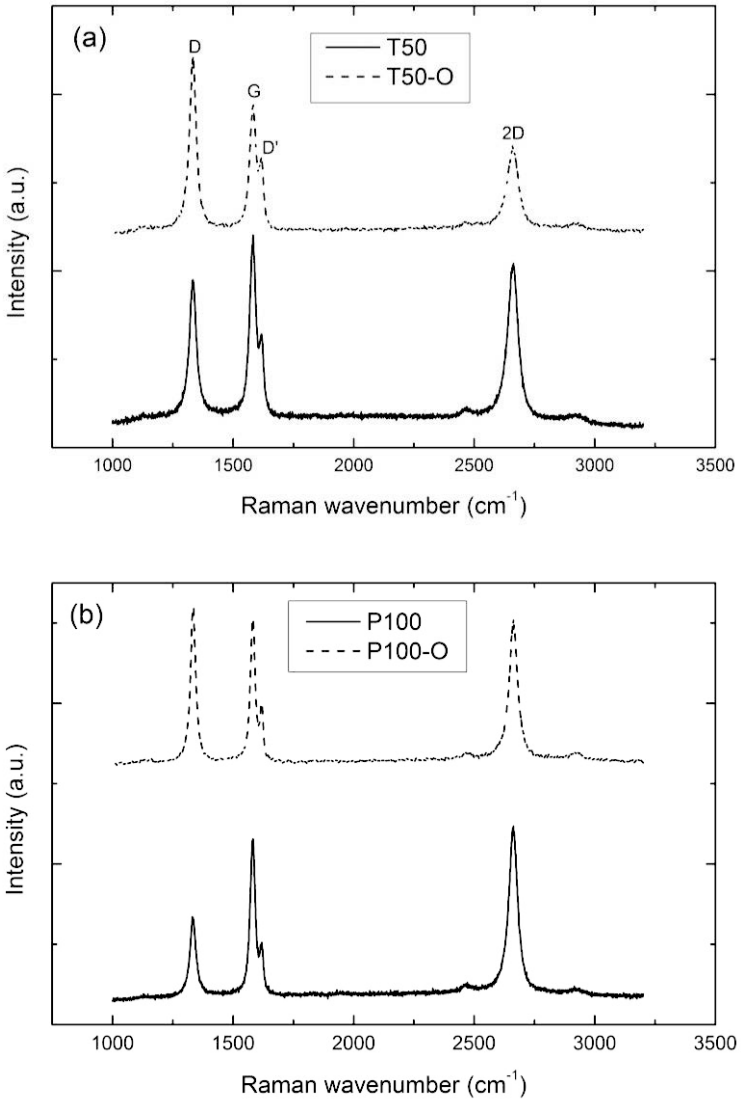

Figure 2.6. Raman spectra of (a) a T50 PAN-based carbon fibres and (b) a P100 pitch-based carbon fibres (untreated (top) and plasma treated (bottom)). (Adapted from Montes-Morán and Young, 2002b with permission from Elsevier).

2.3.2. Stress-induced Raman Band Shifts

The positions of all the Raman bands are found to shift when the carbon fibres are subjected to tensile deformation and this phenomenon can be employed to follow the deformation micromechanics.

Figure 2.7 compares the 2D band of a P100 fibre in the undeformed state and two levels of tensile and compressive strain (0.6% and 0.2% respectively). The band moves towards lower wavenumbers (red shift) when the fibre is in tension, the shift is in the opposite direction (blue shift) when in compression. A significant broadening of the Raman band when the fibre is deformed can be also seen from Figure 2.7. Similar stress-induced Raman band shift behaviour is also found for PAN-based carbon fibres such as T50.

It is found that there is an approximately linear shift of the band position with tensile strain as shown in Figure 2.8 for the 2D band of both the T50 and P100 fibres. Since the fibres deform in an approximately linearly elastic manner there is also a linear shift with stress. It will be shown that Figure 2.8 can be used as a simple calibration to determine the distribution of stress along a fibre using a Raman laser beam focused onto individual fibres inside the matrix resin.

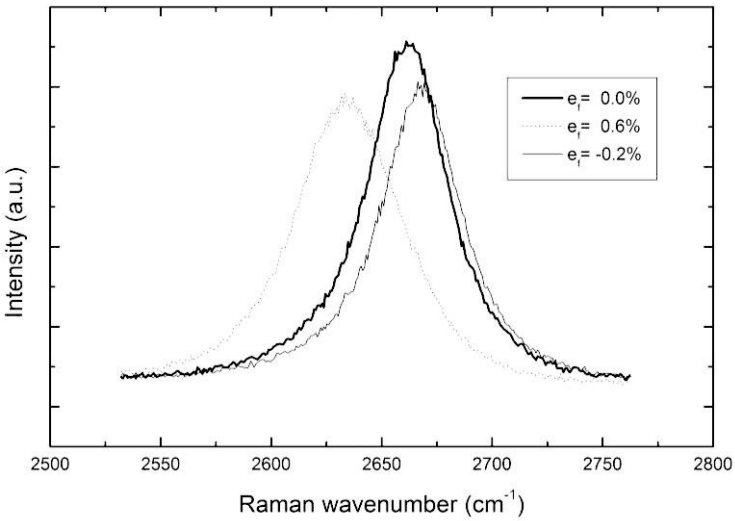

Figure 2.7. Shift of the 2D band peak on the application of tensile and compressive strain to a P100 carbon fibre. (Adapted from Montes-Morán and Young, 2002b with permission from Elsevier).

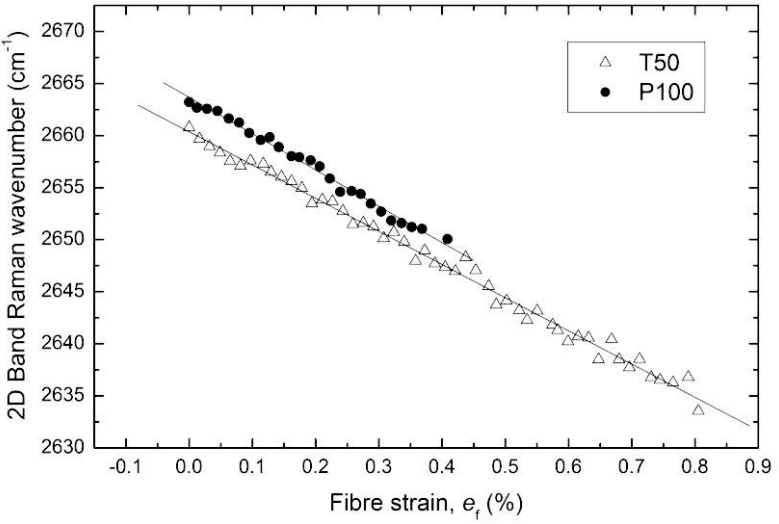

Figure 2.8. Variation of the 2D Raman band peak position with strain in as-received T50 and P100 carbon fibres. (Adapted from Cooper et al. 2001 with permission from Elsevier).

It is also important to point out that it is found that the slope of the lines in Figure 2.8 is found to depend upon the Young's modulus of the carbon fibres (Cooper et al, 2001). This is shown in Figure 2.9 for a number of pitch-based carbon fibres. The measured Raman band shifts of PAN-based carbon fibres are found to fall upon the same line (Young, 1995)

It can be seen that there is an approximately linear dependence of the band shift rate upon the fibre Young's modulus and the slope of the dashed line is of the order of -50 to -60 cm^{-1}/TPa. It is found that this is a universal relationship for the 2D band applicable to all different forms of graphitic carbon materials (Cooper et al, 2001). It is now used widely to follow the deformation behaviour of other types of sp^2 carbon materials such as carbon nanotubes (Deng et al, 2011) and graphene (Young et al, 2012). The rates of Raman band shift (per unit strain) for such materials in nano-composites are found to be proportional to the effective values of their Young's moduli.

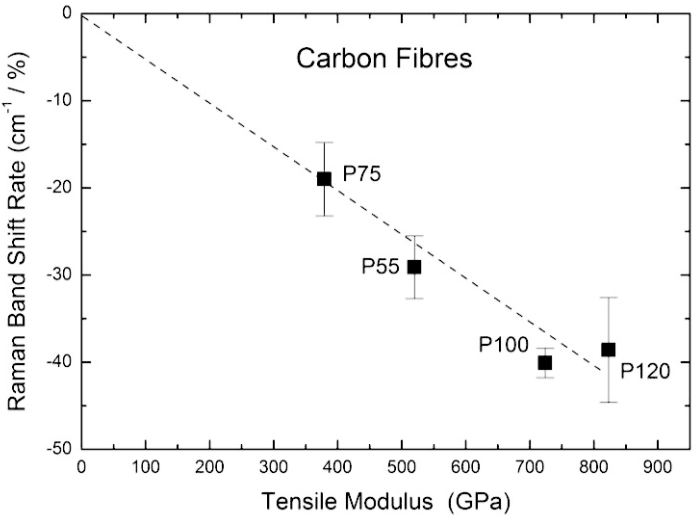

Figure 2.9. Shift rate of the 2D Raman band per unit strain as a function of the tensile Young's modulus for a number of different pitch-based carbon fibres.

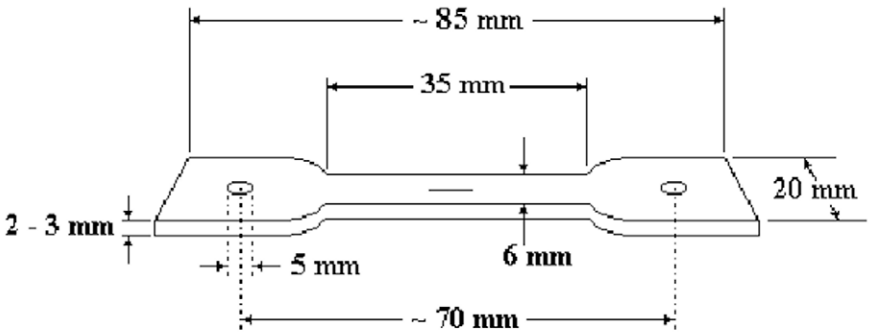

Figure 2.10. Schematic diagram of a model composite specimen containing a single fibre embedded within a transparent polymer resin. The matrix strain is determined by the resistance strain gauge and fibre strain by obtaining Raman spectra along the length of the fibre. (Adapted from Montes-Morán and Young, 2002b with permission from Elsevier).

2.3.3. Analysis of Micromechanics

The fibre stress or strain can be determined from the stress-induced shift of the Raman bands obtained from the fibre using a laser beam focused onto an individual fibre inside the matrix resin as shown in Figure 2.10. The laser beam diameter in a typical modern microscope-based Raman spectrometer is typically ~1 μm. This is significantly smaller than the usual fibre diameter (5-10 μm) which means that fibre stress and strain mapping can now be undertaken at high precision along individual fibres (Montes-Morán and Young, 2002b).

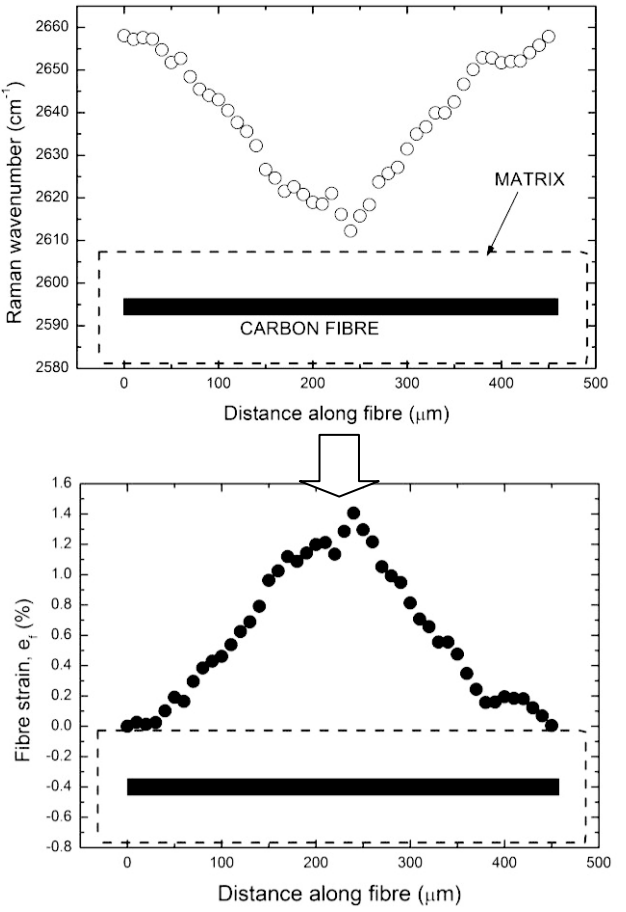

Figure 2.11. Determination of strain from Raman spectra obtained along a carbon fibre. (Adapted from Montes-Morán and Young, 2002b with permission from Elsevier).

Figure 2.11 shows how the strain along a carbon fibre within a matrix can be determined from the local positions of the 2D band in the Raman spectra obtained from the fibre. Well-defined Raman bands can be obtained from the fibres since the Raman scattering from the fibres is generally much stronger than that of the resin matrix. The band shift need to be calibrated first of all by deforming single fibres in air producing data such as those shown in Figure 2.8. The fibre strain can then be readily determined since the bands tend to shift approximately linear with strain.

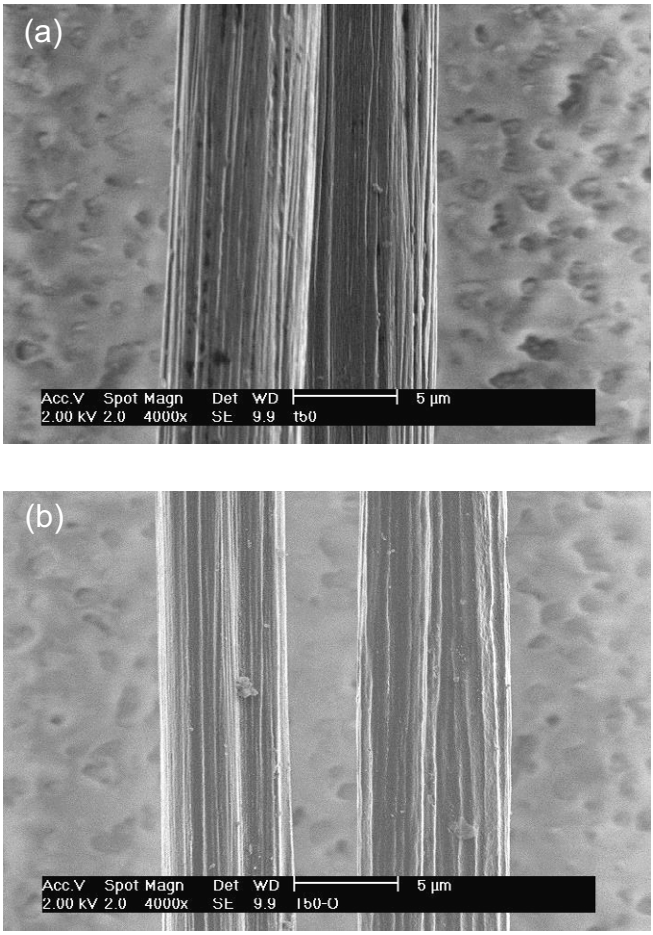

Figure 2.12. Scanning electron micrographs of (a) untreated and (b) plasma-treated T50 carbon fibres. (Adapted from Montes-Morán and Young, 2002a with permission from Elsevier).

2.3.4. Effect of Fibre Surface Treatment

The carbonaceous nature of the surface of carbon fibres leads to low levels of stress transfer from the matrix to the fibres. This lack of fibre/matrix adhesion has been partially overcome with the development of surface treatments that nowadays are implemented fully in the carbon fibre fabrication process. The conventional surface treatment used by carbon fibre manufacturers is an electrochemical oxidation. Apart from the relative success they achieve in the improvement of the interfacial properties of composites, increasing concern about environmental pollution problems has limited wide industrial application of such chemical surface treatments. The development of alternative environmental-friendly methods is an attractive prospect, from both scientific and technological points of view. Among these new methods, the surface modification of fibres by cold plasma is becoming popular and it is now an important branch of plasma technology

High modulus (HM) carbon fibres are possibly one of the most impressive reinforcements of composites in terms of specific tensile properties. These properties are related to the high degree of orientation of the crystallites and this highly graphitic character is also responsible for high level of thermal and electric conductivity. All these properties confer upon HM carbon fibres an unquestionable role in the aerospace industry. On the other hand, the enhanced crystallinity of this type of fibre is often reflected in a lower efficiency of industrial methods for increasing the carbon surface activity, in comparison with the high strength (HT) carbon fibres in that HM carbon fibres are more resistant to electrochemical oxidation than HT ones

The behaviour of untreated and unsized T50 PAN-based HM carbon fibres has been studied by Montes-Morán and Young (2002b). Plasma-treated samples were obtained (-O series) from the as-received fibres. Microwave (2.45 GHz) plasma treatments were carried out in a cylindrical chamber where the fibres were placed during 3 min of residence at 75 W. Yarns of fibres (2k, 20 cm long) were attached to a glass rack, running parallel to the cylinder axis. Oxygen (99.999%) was employed as the activation gas with a chamber pressure of 1.0 ± 0.1 mbar during the treatment time. Such a configuration gave rise to a very homogeneous treatment confirmed by several fibre surface characterisation techniques. Scanning electron micrographs of the two types of fibres are shown in Figure 2.12.

Figure 2.13(a) shows the variation of fibre strain e_f ($= \sigma_f/E_f$) along a T50-O plasma-treated carbon fibre in an epoxy resin subjected to different levels of matrix strain, e_m. The data have been fitted to Equation (2.15) using the aspect ratio of the fibre, s and by choosing appropriate values of n and it can be seen that there is a close correlation between the theoretical curves and experimental data points. Moreover, it can be seen that the strain in the fibre is that same as the matrix strain in the middle of the fibres as was assumed in the theoretical analysis earlier.

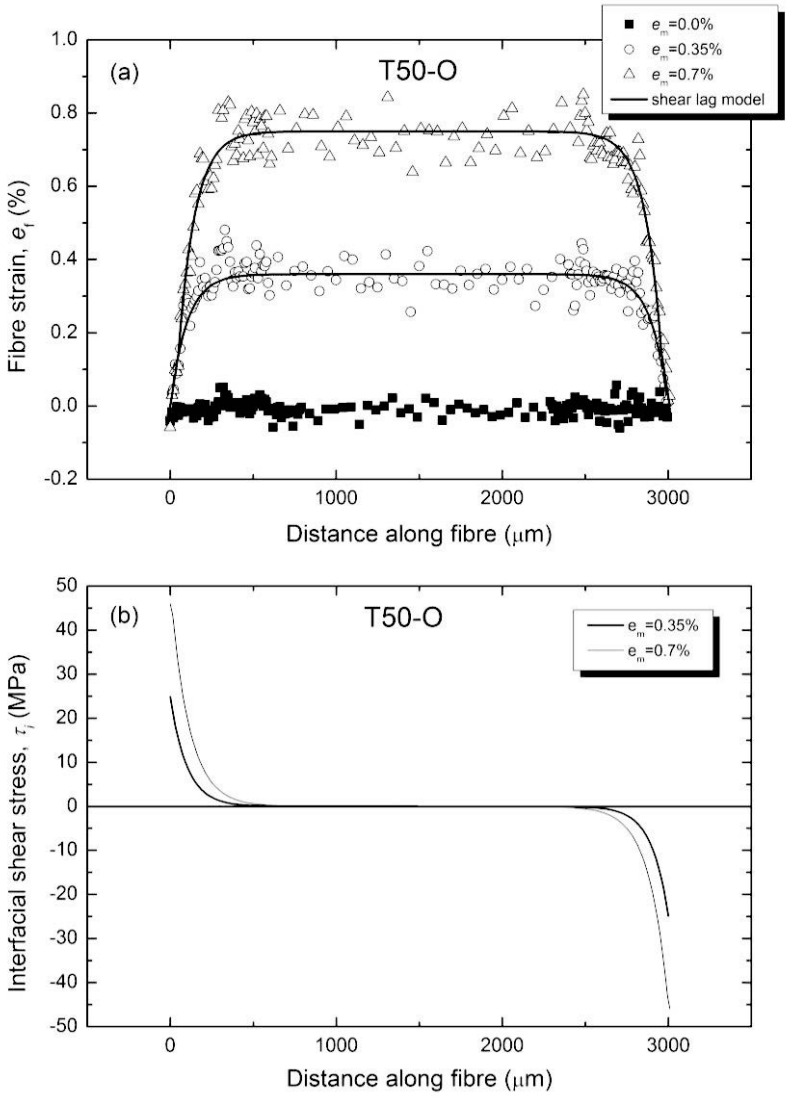

Figure 2.13. (a) Fibre strain distributions determined from strain-induced Raman band shifts at different levels of matrix strain in an epoxy resin for a plasma treated T50-O fibre up to 0.7% strain. (b) Derived distribution of interfacial shear stress along the fibre. (Adapted from Montes-Morán and Young, 2002b with permission from Elsevier).

It should be noted, however, that Equation (2.15) cannot be used to determine n since the value of $\ln(R/r)$ is essentially indeterminate. It is more appropriate to think of n as a fitting parameter that characterises the efficiency of stress transfer between the matrix and fibre (Young and Lovell, 2011). It is possible, however, to determine the distribution of interfacial shear stress τ_i along the fibre as shown in Figure 2.13(b). It can be seen that the interfacial shear stress is highest at the fibre ends (where there is a gradient of fibre strain or stress). For a matrix strain of 0.7% the value increases to around 45 MPa which is approaching the shear yield stress of the resin.

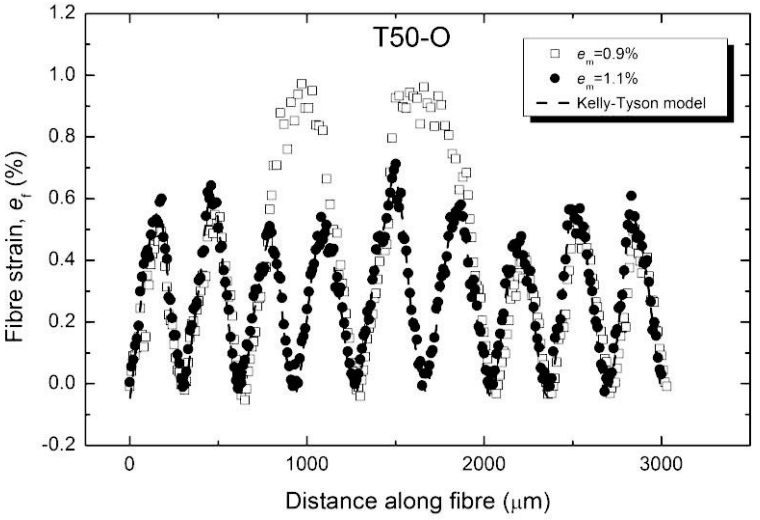

Figure 2.14. Fibre strain distributions determined from strain-induced Raman band shifts at different levels of matrix strain (up to 1.1%) in an epoxy resin for a plasma-treated T50-O fibre showing the effect of fibre fragmentation. (Adapted from Montes-Morán and Young, 2002b with permission from Elsevier).

The effect of increasing the matrix strain to 0.9% is shown in Figure 2.14. At this matrix strain level the T50-O fibre undergoes fragmentation (the strain falls to zero at the fibre breaks) which saturates at a matrix strain of 1.1%. In this case the interfacial adhesion has been lost and stress transfer at the interface is essentially frictional so that there is an approximately triangular variation along the length of each fragment (Kelly and Tyson, 1965). Moreover, it can be seen that the peak fragment strain are well below the matrix strain, indicating that once the fibres have undergone fragmentation reinforcement is diminished.

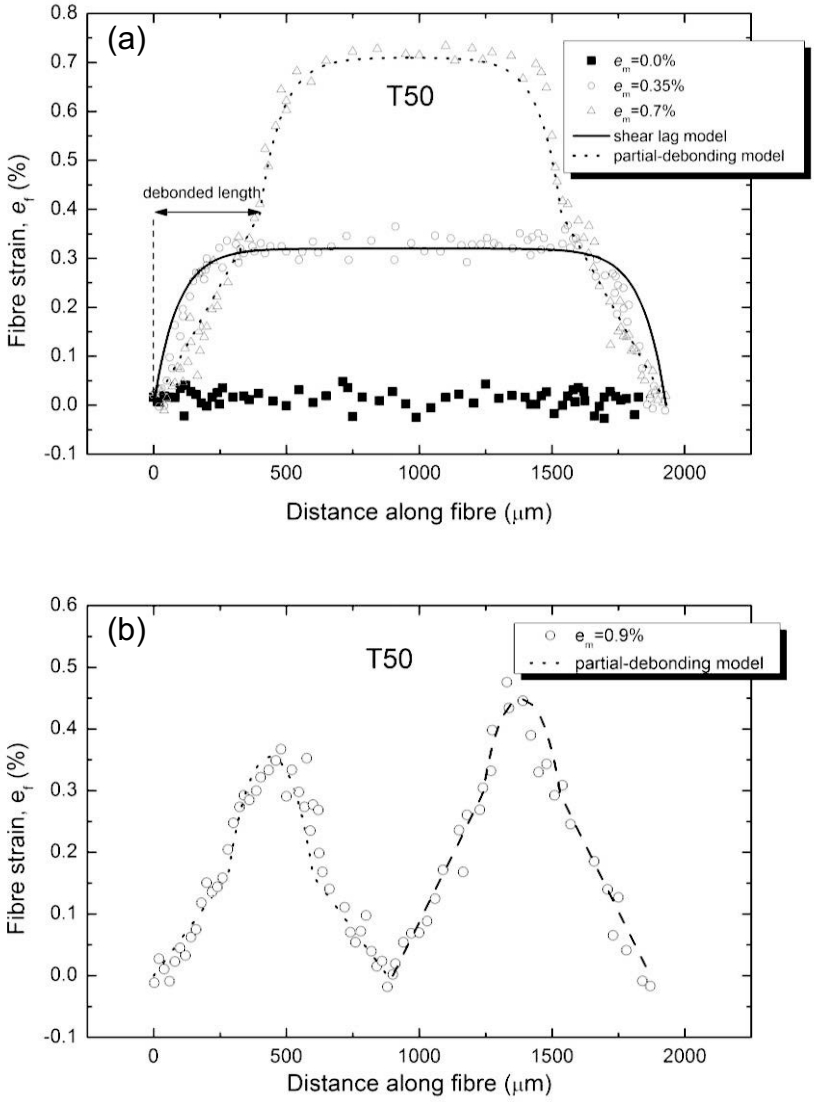

Figure 2.15. Fibre strain distributions determined from strain-induced Raman band shifts at different levels of matrix strain in an epoxy resin for an untreated T50 fibre, showing the effect of debonding at the fibre matrix interface at the higher strain level. (a) Low strain region and (b) high strain region. (Adapted from Montes-Morán and Young, 2002b with permission from Elsevier).

The behaviour of a T50 fibre that had not been modified by plasma treatment is shown in Figure 2.15. The distribution of strain in the fibre at 0.35% matrix strain follows the shear-lag model defined by Equation (2.15). When the matrix strain is increased to 0.7%, however, the distribution of strain is somewhat different with approximately linear behaviour at the two ends. This is an indication that the fibre has undergone debonding that starts at the fibre ends and progresses along the fibre as the level of matrix strain is increased (Montes-Morán and Young, 2002b). This can be compared with the behaviour shown in Figure 2.12(a) for the T50-O fibre at 0.7% strain.

At high strain Figure 2.15(b) shows that the fibre-matrix interface has failed completely and the fibre has broken into two fragments with approximately triangular strain distributions. The length of the two fragments is around 1000 μm (around 1 mm). This is significantly longer than that of the fragments of the T50-O fibre shown in Figure 2.14 which are only around 300 μm long. This is a clear demonstration of the effect of fibre surface treatment upon the micromechanics of deformation.

2.3.5. Interfacial Shear Stress

So far the ability of Raman spectroscopy has been demonstrated for the assessment, in a qualitative manner, of the changes on fibre/matrix adhesion after the plasma treatment of the T-50 HM carbon fibres. It is necessary, however, to quantify such an adhesion enhancement. For a given matrix strain level, the interfacial shear stress, τ_i, at any point along the fibre can be derived from a consideration of the balance of forces at the interface. Equation (2.3) can be recast to give

$$\tau_i(x) = \frac{E_f r}{2} \frac{de_f}{dx} \tag{2.17}$$

where E_f and r are the fibre modulus and radius, respectively, e_f is the fibre strain, and x is the position along the fibre. Since Raman spectroscopic studies of single-fibre composites provide the fibre strain distribution, it makes it also possible to determine the point-to-point variation of the interfacial shear stress using either analytical models or directly from the measured fibre strain distribution.

The maximum value of the interfacial shear stress, $\tau_{i,\,max}$, can be determined directly from plots of the variation of $\tau_i(x)$ with distance along the fibre (e.g. Figure 2.13(b)). Figure 2.16 compares the evolution of $\tau_{i,\,max}$ with applied matrix strain for a T50-O single-fibre/epoxy composite. It can be seen that τ_{max} initially increases with increasing matrix strain and reaches a maximum value of 45 MPa at 0.9% matrix strain. There are basically two possible routes to interface failure in fibre-reinforced composites. Firstly interface failure occurs when $\tau_{i,\,max}$ reaches the interfacial shear strength (IFSS), i.e., the parameter used conventionally to quantify the degree of adhesion between fibre and matrix. Secondly, the interface failure can also occur

when $\tau_{i,\,max}$ reaches the shear yield stress of the matrix, τ_y. The shear yield stress of the matrix used in this study was thought to be around 45 MPa as indicated in Figure 2.16. Hence it appears that the strength of the fibre-matrix interface in the case of the T50-O plasma-treated fibre was limited by the shear yield stress of the matrix. This should be contrasted with similar measurements upon the untreated T50 fibre where $\tau_{i,\,max}$ was found to be only around 20 MPa and its value is controlled by cohesive failure of the fibre-matrix interface (Montes-Morán and Young, 2002b).

In conclusion it is found that the fibre surface treatment increases the value of $\tau_{i,max}$ significantly compared with the untreated fibre but the strength of the interface is eventually limited by shear yielding of the epoxy resin matrix.

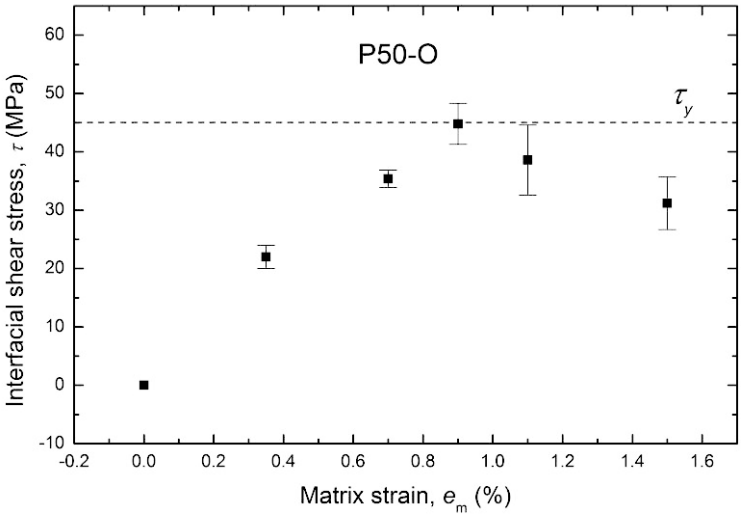

Figure 2.16. Variation of maximum interfacial shear stress $\tau_{i,\,max}$ with applied matrix strain for T50-O fibre/epoxy composite. (Adapted from Montes-Morán and Young, 2002b with permission from Elsevier).

2.4. Conclusions

It has been shown that a relatively simple theoretical analysis can be used to predict the local distribution of stress and strain in a fibre in a composite. Moreover, it has been demonstrated that the local stress or strain distribution can be determined experimentally using Raman spectroscopy and that there is a good correlation between the theoretical and experimental approaches.

It is clear that the issue of reinforcement by a single discontinuous fibre is now well understood but there are still challenges to be addressed in terms of the fundamental mechanics such as developing better analytical methods that do not suffer from some of the issues that arise using the shear-lag approach. There continue to be developments in numerical methods such as finite element analysis and the increasing power of computer systems offers scope for solving even more complex problems.

There are, however, a number of unsolved problems in the field of composite micromechanics that include:

- Fibre compression – the extent to which failure occurs through geometrical instabilities or internal compressive failure processes is still not resolved.
- Effect of fibre orientation and waviness – it is still not fully understood how fibre waviness affects properties especially when a composite is subjected to axial compression.
- Reinforcement with nanofibres and nanotubes – there is no clear indication as yet as to the extent to which the deformation of nanofibres and nanotubes within a composite can be modelled using continuum mechanics. Experience with graphene (Gong et al, 2010) now indicates that it may also be applicable in this case.

There is no doubt that future developments of the theoretical and experimental approaches outlined in this review will enable further significant advances to be made.

References

Cooper C. A., Young R. J., and Halsall M. (2001). Investigation into the deformation of carbon nanotubes and their composites through the use of Raman spectroscopy. *Composites A: Applied Science and Manufacturing*, 32:401-411.

Cox H. L. (1952). The elasticity and strength of paper and other fibrous materials. *British Journal of Applied Physics*, 3:72-79.

Deng L. B., Eichhorn S. J., Kao C. C., and Young R. J. (2011). The effective Young's modulus of carbon nanotubes in composites. *ACS Applied Materials & Interfaces*, 3:433-440.

Gong L., Kinloch I. A., Young R. J., Riaz I., Jalil R., and Novoselov K. S. (2010). Interfacial stress transfer in a graphene monolayer nanocomposite. *Advanced Materials*, 22:2694-2697.

Gibson R. F. (2012). *Principles of Composite Material Mechanics*, 3rd Edition, CRC Press, Boca Raton.

Huang Y., and Young R. J. (1994). Analysis of the fragmentation test for carbon fibre/epoxy model composites using Raman spectroscopy. *Composites Science and Technology*, 52:505-517.

Hull D., and Clyne T. W., (1996). *An Introduction to Composites Materials*, Cambridge University Press, Cambridge.

Kelly A., and Macmillan N. H. (1986). *Strong Solids*, 3rd Edition, Clarendon Press, Oxford.

Kelly A., and Tyson W. R. (1965). Tensile properties of fibre-reinforced metals - copper/tungsten and copper/molybdenum. *Journal of the Mechanics and Physics of Solids*, 13:329-350.

Kelly A. (1966). *Strong Solids*, Clarendon Press, Oxford.

Krenchel H. (1964). *Fibre Reinforcement*, Akademisk Forlag, Copenhagen.

Montes-Morán M. A., and Young R. J. (2002a). Raman spectroscopy study of HM carbon fibres: effect of plasma treatment on the interfacial properties of single fibre/epoxy composites, Part I: Fibre characterization. *Carbon*, 40:845-855.

Montes-Morán M. A., and Young R. J. (2002b). Raman spectroscopy study of HM carbon fibres: effect of plasma treatment on the interfacial properties of single fibre/epoxy composites, Part II: Characterisation of the fibre/matrix interface. *Carbon*, 40:857-875.

Nairn J. A. (1997). On the use of shear-lag methods for analysis of stress transfer unidirectional composites. *Mechanics of Materials*, 26:63-80.

Young R. J. (1995). Monitoring deformation processes in high-performance fibres using Raman spectroscopy. *Journal of the Textile Institute*, 86:360-381.

Young R. J., Kinloch I. A., Gong L., and Novoselov K. S. (2012). The mechanics of graphene nanocomposites: A review', *Composites Science and Technology*, 72:1459–1476.

Young R. J., and Lovell P. A. (2011). *Introduction to Polymers*, CRC Press, Boca Raton. Chapter 24